# Quantized Symmetry of Liquid Monolayer Domains

**Ka Yee C. Lee and Harden M. McConnell***

*Department of Chemistry, Stanford University, Stanford, California 94305*

*Received: June 2, 1993**

Theoretical arguments have been developed that the shapes of lipid domains at the air–water interface can be understood in terms of a competition between line tension and long-range electrostatic forces. These electrostatic forces can be approximated by effective dipoles, that is, the differences in dipole densities $\mu$ in coexisting phases. Recent experimental work has given quantitative confirmation that the long-range electrostatic forces can be expressed in terms of these dipoles. The present work further tests the theory of domain shapes involving competition between line tension and dipolar forces by observations of transitions of circular domains to domains of lower symmetry. These transitions occur when the electrostatic repulsive forces exceed the forces of line tension $\lambda$. Transitions of circular domains to domains with shapes of lower symmetry are functions of domain radius and the dimensionless parameter $\lambda/\mu^2$; the experimental results are in accord with theory to within the experimental error.

## Introduction

Fluorescence microscopy has been used to show that certain binary mixtures of lipids give rise to immiscible liquid phases at the air–water interface.[1-4] The immiscibility of the two liquid phases results in a monolayer with domains of one liquid interspersed in a two-dimensional sea of the other. The domain shapes and sizes in these lipid mixtures have been interpreted phenomenologically in terms of a competition between line tension at the domain boundary and dipole–dipole electrostatic repulsion between molecules within and between domains.[5-12] Line tension acts to minimize the length of the interface between the two liquid phases and thus favors compact domain shapes. The electrostatic repulsive force tends to maximize the distance between molecules within a domain and thus favors noncircular domain shapes.

Based on this line tension-equivalent dipole picture, a number of theoretical studies have been carried out to model shape transitions of lipid monolayer domains at the air–water interface.[7-13] Earlier work gives a thermodynamic equilibrium size for a circular lipid domain.[8] As the domain size increases beyond this equilibrium value, a point is reached when it becomes unstable with respect to distortion to a shape with 2-fold symmetry.[7,8] As the size further increases, the domain becomes unstable with respect to higher harmonic distortions.[9] For a very large domain, the domain boundary appears straight to short-wavelength harmonic distortions. A dynamical stability analysis has recently been performed for the straight edge of a large domain.[12] There have been a number of experimental studies of shape instabilities and shape relaxation dynamics of domains in Langmuir films at the air–water interface.[3,13,14] However, there still lacks experimental results that thoroughly test the theoretical model for lipid monolayer domain shape transitions.

The present work involves both theoretical and experimental aspects of shape transitions of domains. On the theoretical side, we extend the shape transition analysis of circular domains to higher-order harmonic distortions.[9] Comparison is made with the straight edge instability analysis;[12] both give identical results in the limit of high harmonics. The shapes of lipid domains bear a strong resemblance to those found in quasi-two-dimensional domains of ferrofluids in transverse magnetic fields.[15,16] Recently, Langer *et al.* examined the dynamics of labyrinthine pattern formation in these systems by developing a formalism for the description of the dissipative motion of closed curves while conserving area.[17] A comparison between our calculations and those of Langer *et al.* is given in the Appendix.

The motivation behind this experimental work has been to test the validity of the theoretical model, by examining how well it accounts for observed shape transitions. We have accordingly employed a binary mixture of dihydrocholesterol (DChol) and dimyristoylphosphatidylcholine (DMPC) that forms two immiscible liquid phases at certain temperatures and pressures; one phase is rich in DChol, and the other phase is rich in DMPC.[18] This system is ideal for testing the model for shape transitions since (i) all molecular dipoles are on average perpendicular to the monolayer surface and (ii) the lipid-phase composition, and thus the line tension, can be changed by altering the monolayer surface pressure. However, one difficulty for such experimental studies is that the domains spontaneously formed at the air–water interface upon spreading are typically a few microns in size. We circumvent this by utilizing a special technique yielding lipid domains of large size. Our experiments use these large domains to study the shape transitions. Comparisons of the experimental findings and the theoretical model are then possible.

## Background Theories

Consider an isolated, circular lipid domain of radius $R_c$ in the $xy$ plane. As in previous work, it is assumed that the molecular dipoles within as well as outside the domain are vertically oriented in the $z$ direction.[9] This approximation is most accurate for liquid domains surrounded by a second liquid. The shape-dependent energy of this domain is a sum of an electrostatic energy $F_{el}$ and a line tension energy $F_\lambda$,[7,8]

$$F = F_{el} + F_\lambda \tag{1}$$

The two energies are

$$F_{el} = -\frac{\mu^2}{2}\oint\oint\frac{d\vec{R}\cdot d\vec{R}'}{r} \tag{2}$$

$$F_\lambda = \oint \lambda \, dR \tag{3}$$

Here, $\mu$ is the difference in dipole densities between the two phases, and $\lambda$ is the effective line tension given by

$$\lambda = \lambda_0 - \mu^2 \tag{4}$$

with $\lambda_0$ a hypothetical line tension in the absence of dipolar forces.[19] For a circular domain of fixed area $A = \pi R_c^2$, the total energy

* Abstract published in *Advance ACS Abstracts*, September 1, 1993.

0022-3654/93/2097-9532$04.00/0 

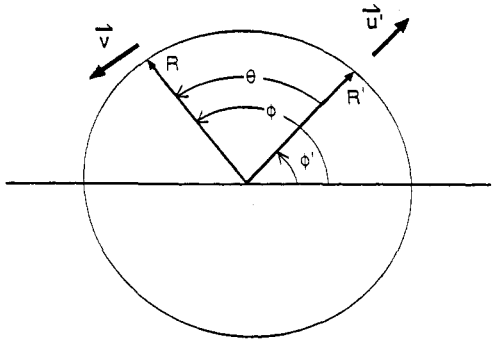


**Figure 1.** Cylindrical coordinates used for the calculations. The unit vectors $\vec{u}$ and $\vec{v}$ (and $\vec{u}'$ and $\vec{v}'$) are parallel and perpendicular to the radius vector $\vec{R} = \vec{u}(R_0 + \rho)$ and $\vec{R}' = \vec{u}'(R_0 + \rho')$, where $\rho = r_n \cos n\phi$ and $\rho' = r_n \cos n\phi'$.

$F$, is then

$$F = -2\pi R_c \mu^2 \ln \frac{8R_c}{e^2\Delta} + 2\pi\lambda R_c \tag{5}$$

where $\Delta$ can be interpreted as the distance of separation of neighboring dipoles. The radius of a circular domain that minimizes the energy of the system is[8]

$$R_{eq} = \frac{e^3\Delta}{8} e^{\lambda/\mu^2} \tag{6}$$

Circular domains with larger radii are unstable with respect to harmonic shape distortions.[9-11] For instance, when the radius equals, or exceeds $R_2$, where[7,9]

$$R_2 = \frac{e^{10/3}\Delta}{8} e^{\lambda/\mu^2} \tag{7}$$

the circular shape is unstable with respect to a transition to a shape with 2-fold symmetry. The radius $R_n$ at which the circular shape becomes unstable with respect to a transition to a shape with $n$-fold symmetry is[9]

$$R_n = \frac{e^{Z_n}\Delta}{8} e^{\lambda/\mu^2} \tag{8}$$

The term $Z_n$ in eq 8 has a complicated dependence on $n$, which makes difficult the evaluation of $R_n$ for arbitrary $n$. The same shape transitions can be brought about by keeping the domain radius fixed while changing surface pressure. This alters the value of $\lambda/\mu^2$, since for this two-phase system the composition of the phases depends on the surface pressure.

Domains of infinite radii are unstable with respect to a wide range of spatial frequencies. Here one may consider the straight edge of an infinite domain to study shape transitions. This straight edge is unstable with respect to harmonic distortions for all spatial frequencies $k$ that are less than a critical frequency, $k_{co}$, given by[12]

$$k_{co} = \left[\frac{\Delta}{2} e^{(1+2C)/2} e^{\lambda/\mu^2}\right]^{-1} \tag{9}$$

where $C \approx 0.577\,215$ is the Euler constant. The harmonic mode that grows most rapidly has a spatial frequency, $k_{mo}$, related to $k_{co}$ by[12]

$$k_{mo} = k_{co}/e^{1/3} \tag{10}$$

**Instability of a Circular Domain**

Following a previous calculation,[9] we consider the circular domain of radius $R_c$ in Figure 1 with a single-mode harmonic distortion of the form

$$\rho = r_n \cos n\phi \tag{11}$$

where $r_n$ is the amplitude of the distortion. The electrostatic energy in eq 2 can then be expressed as follows:

$$F_{el} = -\frac{\mu^2}{2}\int_0^{2\pi} d\phi' \int_0^{2\pi} d\phi \frac{(d\vec{R}/d\phi)\cdot(d\vec{R}'/d\phi')}{G} \tag{12}$$

where

$$\vec{R} = \vec{u}(R_0 + \rho) \tag{13}$$

$$G = \{2[R_0^2 + R_0(\rho + \rho') + \rho\rho'][1 - \cos\theta] + (\rho - \rho')^2 + \Delta^2\}^{1/2} \tag{14}$$

$$\theta = \phi - \phi' \tag{15}$$

In this analysis, it is necessary to maintain the total area of the domain constant. Thus, to second order

$$R_0^2 = R_c^2 - r_n^2/2 \tag{16}$$

The electrostatic energy that is quadratic in $r_n$ is

$$F_{el}^{(2)} = -\mu^2\left[\frac{\pi r_n^2 n^2}{2R_c} + \frac{\pi r_n^2}{2R_c}\int_0^{\pi} d\theta Y X^{-1}\right] \tag{17}$$

where

$$Y = -\frac{3}{4}\cos\theta + \frac{1}{2}\left[(n)(n+1) + \frac{1}{4}\right]\cos(n+1)\theta + \frac{1}{2}\left[(n)(n-1) + \frac{1}{4}\right]\cos(n-1)\theta - \frac{1}{2}\frac{(1 - \cos n\theta)\cos\theta}{1 - \cos\theta} \tag{18}$$

$$X = \left(x + \frac{1}{2(1 - \cos\theta)}\right)^{1/2} \tag{19}$$

$$x = \Delta^2/4H^2 \tag{20}$$

$$H = \left[R_0^2 + R_0(\rho + \rho') + \rho\rho' + \frac{(\rho - \rho')^2}{2(1 - \cos\theta)}\right]^{1/2} \tag{21}$$

The various terms in the integrand of eq 17 can be recombined into two types of integrals, $V(x)$ and $L_n(x)$, where

$$V(x) = \int_0^{\pi} d\theta X^{-1} \tag{22}$$

$$L_n(x) = \int_0^{\pi} d\theta (1 - \cos n\theta) X^{-1} \tag{23}$$

Formulas for these integrals are given by Thiele.[20] For the case of interest to monolayer domains, $x \ll 1$, and

$$V(x) = \ln(16/x) \tag{24}$$

$$L_1(x) = 4 \tag{25}$$

Other values of $L_n$ are obtained from the recursion relation for $x \ll 1$

$$L_{n+1} = \frac{1}{2n+1}[4nL_n - (2n-1)L_{n-1}] \tag{26}$$

The second-order term in the electrostatic energy in eq 17 is

$$F_{el}^{(2)} = -\frac{\pi\mu^2 r_n^2}{2R_c}\left[n^2 + \sum_{q=1}^{n+1} a_q L_q + \frac{n^2 - 1}{2}V(x)\right] \tag{27}$$

The term quadratic in $r_n$ from the contribution of the line tension to the energy is obtained from eq 3,

$$F_\lambda = \int_0^{2\pi}\lambda\left(R^2 + \left(\frac{dR}{d\theta}\right)^2\right)^{1/2} d\theta \tag{28}$$

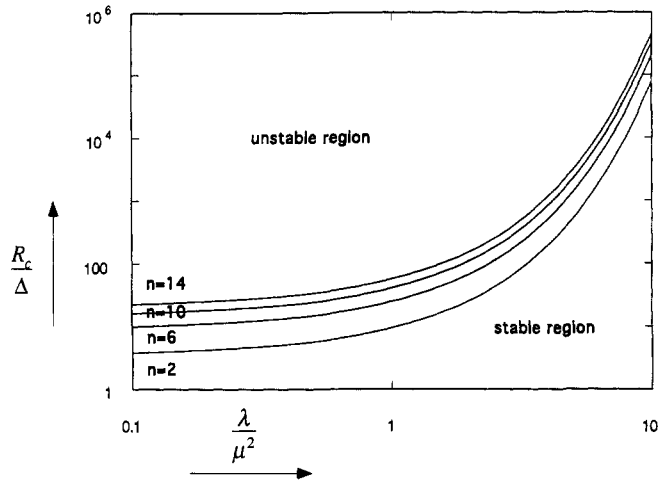


**Figure 2.** Diagram illustrating the critical modes for instabilities of circular lipid monolayer domains obtained by linear stability analysis. The dimensionless radius of the circular domain, $R_c/\Delta$, is plotted against the dimensionless parameter $\lambda/\mu^2$ for the onset of the different modes of instability. Equations 8, 31, and 32 are used to plot the curves for different modes $n$. For equivalent values of the parameters, these results are very close to those obtained by Langer *et al.*[17]

The result is

$$F_\lambda^{(2)} = \frac{\pi\lambda r_n^2}{2R_c}(n^2 - 1) \tag{29}$$

For all small values of $r_n$, the condition on $R_c$ for the $n$-fold shape transition is

$$F_\lambda^{(2)} + F_{el}^{(2)} = 0 \tag{30}$$

The radius $R_n$ for which the circular shape is unstable with respect to a transition to a shape with $n$-fold symmetry is then found to be eq 8, with

$$Z_n = -[n^2 + \sum_{q=1}^{n+1} a_q L_q]/[n^2 - 1] \tag{31}$$

The summation in eq 31 for any value of $n$ can be obtained if the general formulas for $a_q(n)$ are known. The latter are obtained by gathering coefficients of $(1 - \cos n\theta)X^{-1}$ in the integrand of eq 17, and the resulting general form is found to be

$$a_q(n) = \begin{array}{lll} 0.75 + (n-q) & & 1 \\ n-q & & 2 \ldots n-2 \\ -0.5[n(n-1) + 0.25] + 1 & \text{for } q = & n-1 \\ 0.5 & & n \\ -0.5[(n+1)n + 0.25] & & n+1 \end{array} \tag{32}$$

For any value of $\lambda/\mu^2$, the radius $R_n$ at which the circular domain shape becomes unstable with respect to any arbitrary $n$-fold distortion is calculated using eqs 8, 25, 26, 31, and 32. Figure 2 shows the results of this stability analysis whereby lines delineating the stable from the unstable regions for different $n$-harmonic shape transitions are plotted as a function of the domain size and the dimensionless parameter $\lambda/\mu^2$.[21] The figure shows that, for a given domain radius or a given value of $\lambda/\mu^2$, the $n = 2$ mode is always the first to become unstable when increasing the radius or the surface pressure (thus decreasing $\lambda/\mu^2$).

Define a critical spatial frequency for $n$-fold distortions,

$$k_{cn} = \frac{2\pi}{2\pi R_n/n} = \frac{n}{e^{(Z_n-3)}R_{eq}} \tag{33}$$

whereby a circular domain is unstable for all spatial frequencies

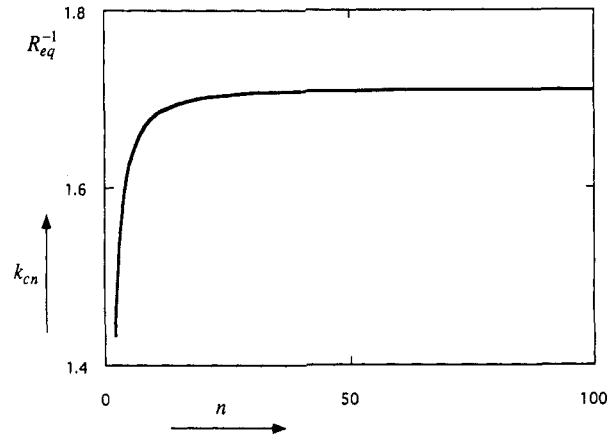


**Figure 3.** A log–log plot of the critical spatial frequency $k_{cn}$ (in units of $R_{eq}^{-1}$) as a function of the instability mode $n$. The critical spatial frequency approaches an asymptotic value given by eq 34 as $n$ becomes large.

$k < k_{cn}$. The variation of this critical spatial frequency as a function of $n$ is depicted in Figure 3. The critical frequency reaches an asymptotic value as $n$ gets large. Numerical calculations using eqs 31–33 show that this value is given by

$$k_{cn}|_{n\to\infty} = (0.585R_{eq})^{-1} \tag{34}$$

For very large $n$, the radius of the domain is large compared to the wavelength of the harmonic distortions. The circular edge of a domain can then be approximated by a straight edge. Equation 9 gives the critical spatial frequency found earlier for a straight edge.[12] This critical spatial frequency can be reexpressed in terms of the equilibrium domain radius, $R_{eq}$, as follows:

$$k_{co} = (4e^{C-2.5}R_{eq})^{-1} = (0.585R_{eq})^{-1} \tag{35}$$

The results in eqs 34 and 35 are equivalent.

### Kinetics of Instability

The foregoing calculations give the range of values for the critical spatial frequencies for harmonic distortions corresponding to instability of a circular domain. A kinetic analysis is required to determine which mode grows most rapidly and thus the mode that should be observed experimentally. We model the competing forces of electrostatics, line tension, and hydrodynamic drag by considering lipid motion in a two-dimensional sheet, which is coupled to a water subphase via a drag coefficient $\gamma$(force/velocity·area).

We assume that the lipid motion is irrotational and that the fluid is incompressible.[22] The velocity potential, $\varphi$, satisfying the equation of motion for an incompressible two-dimensional fluid is

$$\varphi = -\frac{\nu R_c}{n}\left(\frac{r}{R_c}\right)^n \cos n\theta \quad \text{for } r \le R_c \tag{36}$$

$$\varphi = -\frac{\nu R_c}{n}\left(\frac{R_c}{r}\right)^n \cos n\theta \quad \text{for } r > R_c \tag{37}$$

These velocity potentials have been used to describe two-dimensional waves in a circular section of a cylindrical column.[23] The velocity $\vec{v}$ corresponding to $\varphi$ in eqs 36 and 37 satisfies the boundary condition at the edge of the circle ($r = R_c$) for $r_n = 0$ and goes to zero at the origin as well as at infinity. The velocity is related to the magnitude of the harmonic distortion by

$$\frac{\partial r_n}{\partial t} = -\frac{\partial \varphi}{\partial r} \tag{38}$$

The rate of energy loss for the domain shape per solid angle is

$$\frac{1}{2\pi}\left(2r_n\frac{dr_n}{dt}\right)\left(\frac{\partial}{\partial r_n^2}F_n\right) \quad (39)$$

where $F_n$ is the shape-dependent energy associated with a circular domain with harmonic distortions of mode $n$, given by

$$F_n = \pi r_n^2 K_n = -\frac{\pi\mu^2 r_n^2}{2R_c}\left[n^2 + \sum_{q=1}^{n+1} a_q L_q + \frac{n^2-1}{2}V(x)\right] + \frac{\pi\lambda r_n^2}{2R_c}(n^2-1) \quad (40)$$

$K_n$ in eq 40 is the restoring force constant for mode $n$. The initial time-dependent behavior of the instability amplitude $r_n$ is obtained by equating the above rate of energy loss to the rate of viscous energy dissipation. The energy dissipation is due to the water subphase; energy loss due to the monolayer viscosity itself has been shown to be negligible.[24,25] The drag force is assumed to be proportional to the local monolayer velocity, and the rate at which energy is dissipated (per solid angle) is

$$\frac{2n}{2\pi}\left(\int_0^{R_c} r\,dr + \int_{R_c}^{\infty} r\,dr\right)\int_0^{\pi/n} d\theta\,\gamma(\nabla\varphi)^2 = \gamma\left(\frac{dr_n}{dt}\right)^2 R_c^2\left(\frac{1}{2n}+\frac{1}{2n}\right) \quad (41)$$

Fluid flow inside and outside of the domain give equal contributions to the energy dissipation. By eqs 39 and 41, we obtain

$$\frac{1}{r_n}\frac{dr_n}{dt} = -\frac{nK_n}{\gamma R_c^2} \quad (42)$$

The time-dependent behavior of $r_n$ is therefore

$$r_n = A_n \exp\left[-\frac{nK_n}{\gamma R_c^2}t\right] \quad (43)$$

where $A_n$ is a fluctuation amplitude. That is, at time $t = 0$ it is assumed that each mode is thermally excited to a small amplitude $A_n$, but when $t > 0$ the most rapidly growing mode develops an amplitude that exceeds all others.

According to eq 43, the fastest growing mode, $n^*$, for a domain of radius $R_c$ is the one which has the largest coefficient in the exponent (i.e., the lowest value for the term $nK_n$). We have evaluated this for domains of different sizes, each for modes 2 $\leq n \leq$ 25. The results of this calculation are shown in Figure 4a. Each curve depicts how the term $n\pi K_n/\mu^2$ changes with respect to $n$ for a domain of a certain size. The intersection of one of these curves and the $x$ axis gives the critical mode for the domain, whereas the lowest point of the curve indicates its fastest growing mode. In these calculations the mode that grows most rapidly for a domain of a given size is not the mode that has the lowest energy. A plot of the term $\pi K_n/\mu^2$ versus mode number is shown in Figure 4b for domains of the same sizes as in Figure 4a. Comparison of the two figures reveals that the mode with the lowest energy for a domain of a given size has a lower $n$-fold symmetry than the fastest growing mode, which in turn has a lower symmetry than the critical mode. Figure 5 shows how the critical mode, the fastest growing mode, and the lowest energy mode vary with domain size. The data points for the fastest growing mode, $n^*$, fall approximately on the line $n^* = ne^{-1/3}$, while the data points for the lowest energy mode, $n_{le}$, fall approximately on the line $n_{le} = ne^{-1/2}$ as $n$ gets large. Using eq 33, one can then deduce that the spatial frequency of the fastest growing mode, $k_{mn}$, is approximately related to that of the critical

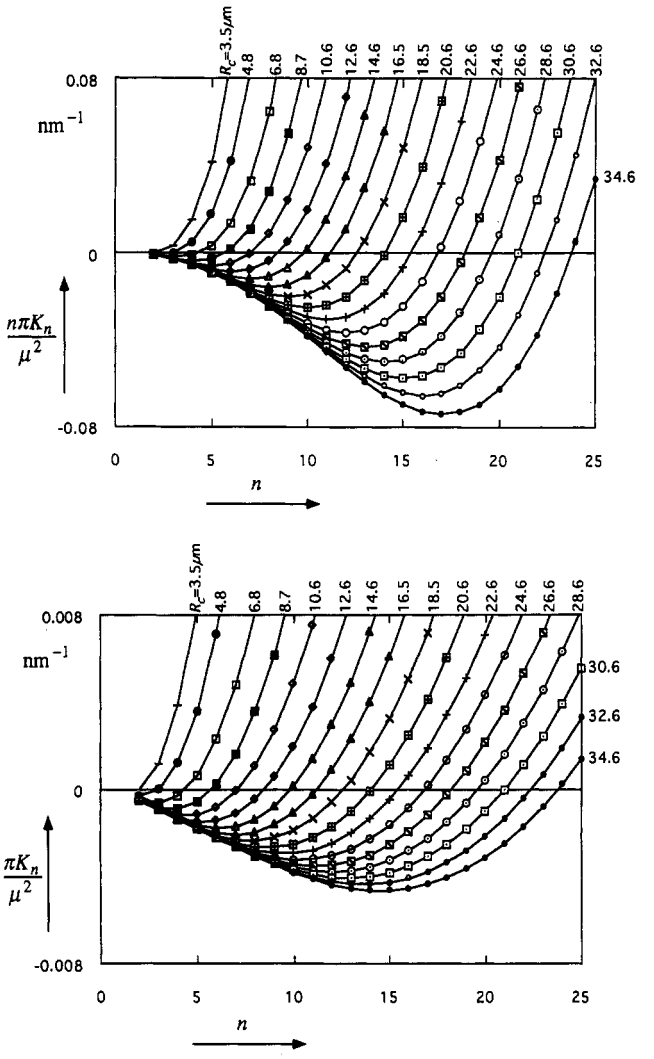


**Figure 4.** Diagrams illustrating how the time constants for the growth rates of harmonic distortions for lipid domains of different radii vary as a function of the mode of instability $n$. The term $n\pi K_n/\mu^2$, which differs from the exponential temporal coefficient in eq 43 by a negative multiplicative constant for a domain of a given size, is used for plot a (top); the term $\pi K_n/\mu^2$, which differs from the exponential temporal coefficient in eq 48 by the same multiplicative constant, is used for plot b (bottom). For a domain of a given radius, the critical mode of instability is the one where the time constant for the growth rate is zero; the fastest growing mode is the one that has the lowest value for the term $n\pi K_n/\mu^2$ (i.e., the highest growth rate) as shown in plot a; and the lowest energy mode is the one that has the lowest value for the term $\pi K_n/\mu^2$ as shown in plot b. The radii shown range from 3.5–35 μm, which are of the same range as the domain radii used in our experiments for the observation of shape transitions via fluorescence microscopy. The distance of separation of neighboring dipoles Δ and the dimensionless parameter $\lambda/\mu^2$ were set equal to 0.9 nm and 7, respectively, for the calculations.

mode, $k_{cn}$, by

$$k_{mn} \approx k_{cn}/e^{1/3} \quad (44)$$

which is similar to the calculation made for an infinite domain with a straight edge (see eq 10).

## Methods and Materials

The experimental setup shown in Figure 6 is similar to that used by Klingler and McConnell.[26] A small Teflon Langmuir trough of dimensions 10 cm × 6 cm is used to hold the monolayer, monitor the surface pressure, and observe shape transitions of lipid domains. The trough has a deeper side (2 cm) and a shallower side (1 cm). The former is used in conjunction with a plunger, which allows for the adjustment of the water level with a precision of about 1 μm. The latter, supporting a smaller depth of the

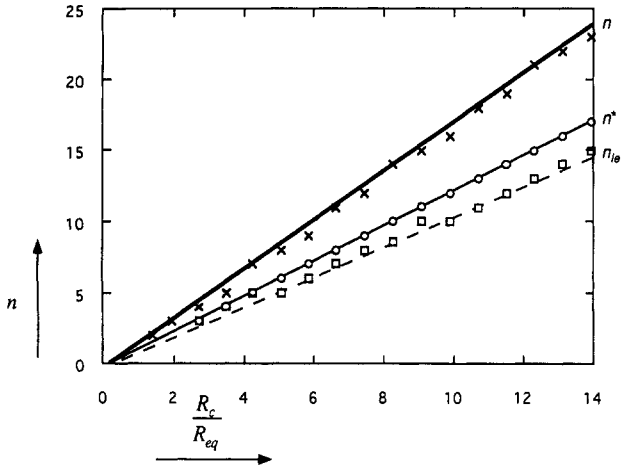


**Figure 5.** Critical, fastest growing, and lowest energy modes as a function of domain radius. The thick solid line joins the critical modes, which are the unstable modes with the largest $n$, calculated using eqs 8, 31, and 32. The thin solid line is a factor of exp(1/3) below the thick solid line; the dotted line is a factor of exp(1/2) below the thick solid line. The crosses, the circles, and the squares indicate integral values of the critical, fastest growing, and the lowest energy modes obtained from calculations shown in Figure 4a,b. The crosses fall on or below the thick solid line because the intersections between the curves and the $x$ axis in Figure 4 do not necessarily correspond to an integral mode number; the highest frequency allowed mode closest to the intersection is taken as the critical mode. The lowest energy modes shown also represent the fastest growing modes obtained from eq 48 when the $1/n$ dependence is omitted in the energy disspation term (see Appendix). The circles fall exactly on the line $n^* = n/\exp(1/3)$ because the radii of the domains in Figure 4 were picked to produce this result.

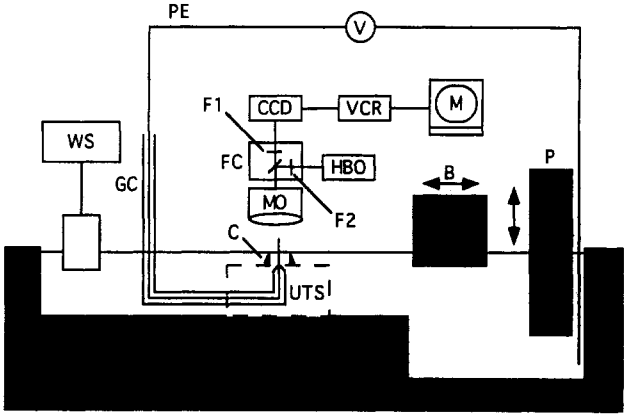


**Figure 6.** Schematics of the experimental setup: B, barrier; C, collar; CCD, CCD camera; FC, fluorescence condenser; F1, 546-nm light filter; F2, >590-nm light filter; GC, glass capillary; HBO, halogen burner; M, monitor; MO, microscope objective; P, plunger; PE, platinum electrodes; UTS, U-shaped Teflon spacer; V, voltage supply; VCR, video cassette recorder; WS, Wilhelmy system.

subphase, helps reduce convection and hence the drift of the film. To further reduce the subphase height, a U-shaped piece of solid Teflon (0.5 cm in height) is placed directly beneath the point of viewing. The entire trough is mounted on a $xy$ translational stage. The surface pressure of the system is monitored using a Wilhelmy film balance with a piece of filter paper attached to a calibrated linear variable differential transformer.

The trough is encased in a housing made of plexiglas, which inhibits air circulation and monolayer drift. We have also incorporated the use of a steel collar in the setup, with which the drift of the monolayer can be virtually eliminated by carefully lowering the water level until the monolayer is caught on the circular edge of the collar.[26] Even when the film is caught at the edge, it is still continuous: any change in surface pressure brings about the same kind of change to lipid domains caught inside and those that are outside the collar.

A binary mixture of L-$\alpha$-dimyristoylphosphatidylcholine (DMPC) and dihydrocholesterol (DChol) is known to form two immiscible liquid phases.[18] The phase diagram of the system has recently been mapped out; shape transitions occur at surface pressures just below the critical mixing–demixing pressure.[18]

Monolayers of 84 mol % DMPC and 15 mol % DChol, with 1 mol % of the dye $N$-(Texas Red sulfonyl)dipalmitoyl-L-$\alpha$-phosphatidylethanolamine (TR-DPPE) added, were spread from a 1-mM solution of 9:1 hexane/ethanol. DMPC was purchased from Avanti Polar Lipids; DChol was purchased from Sigma. The fluorescent lipid probe TR-DPPE was purchased from Molecular Probes. All compounds were used without further purification. Experiments were carried out at room temperature on a subphase of distilled, deionized water.

The monolayer was observed either directly using a Zeiss Photomicroscope III with a Nikon 40X long-distance microscope objective or with a Cohu low-light-level video camera connected to the microscope. The monolayer was illuminated with green light obtained by passing white light through a 546-nm interference filter and observed in the red with a long-pass filter for wavelengths >590 nm. Video images of the monolayer were recorded with a JVC S-VHS BR601MU recorder.

The effect of an inhomogeneous electric field on lipid domains has been reported earlier by Heckl *et al.*[27] Here, we formed large lipid domains by fusing small domains in the presence of a controlled electrical field. A 125-$\mu$m-diameter platinum wire with a rapid taper tip and glass insulation, purchased from Longreach Scientific Resources, was further insulated with varnish. For easier manipulation of the platinum wire, it was epoxied into a hook-shaped glass capillary, with the taper tip sticking out at one end of the capillary and the blunt end of the wire out of the other. This platinum wire assembly was inserted in the aforementioned U-shaped teflon piece as shown in Figure 6. The wire was so placed that approximately 50 $\mu$m of the tapered tip protruded out of the water surface and centered in the viewing field under the microscope. The other end was connected to a power supply, which, in turn, was connected to the water subphase via a platinum counter electrode. Upon application of a dc voltage (up to 120 V) across the platinum electrodes, the protruding part acted as an antenna. Due to the difference in dipole moment densities between the two liquid phases, domains of one phase were attracted or repelled, depending on the polarity of the field applied. An attractive polarity for the DChol-rich phase was first applied, which resulted in the fusion of the dark liquid domains around the platinum tip. When enough material was gathered, the polarity of the electric field was reversed, thus repelling the fused domains and forming a large DChol-rich domain in a background of the DMPC-rich liquid phase.

## Experiments and Results

As discussed earlier, shape transitions can be brought about by either increasing the domain size at a fixed surface pressure or altering the dimensionless parameter $\lambda/\mu^2$ through changes in the surface pressure for a domain of a fixed size. Only a very small surface pressure change is necessary to alter domain composition and bring about a shape transition 1-fold higher in symmetry ($n$-fold to $(n + 1)$-fold). It is therefore difficult to reproduce the identical surface pressure conditions for quantitative comparisons of shape transitions for domains of various sizes in different experiments.

A quantitative study was carried out by observing and comparing shape transitions undergone by domains of different sizes at the same surface pressure. Several domains with radii ranging from 5 to 50 $\mu$m were created and monitored concurrently using the technique described in the previous section. The only variable in the experiment was the domain size. The surface pressure was then slowly increased until shape transitions of the different domains were observed. The harmonicity and the size

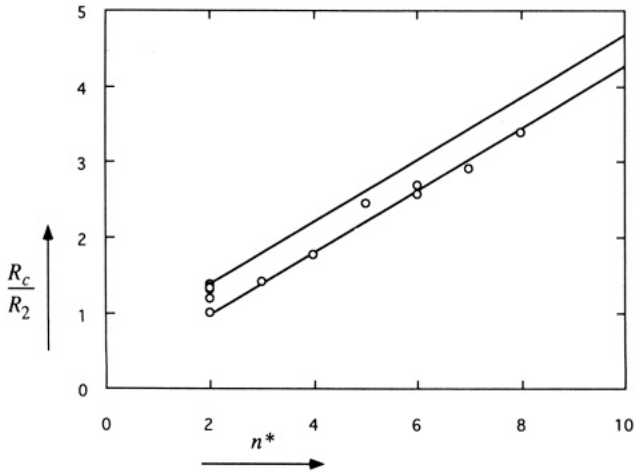


**Figure 7.** Diagram illustrating how the sizes of experimentally observed domains with $n^*$-fold distortions correspond to the theoretically calculated ones for harmonic shape transitions, where $n^*$ is the symmetry number of the fastest growing mode. The two solid lines delineate theoretical zones of $n^*$-fold distortions; the plotted data points are obtained from four sets of experiments. For each set of experiment, domains of different sizes were made and the system was kept at a particular surface pressure. The domains were observed to undergo different $n^*$-fold shape transitions according to their sizes. All experimentally observed domain radii are scaled to $R_2$, the radius at which the circular shape becomes unstable to 2-fold distortions.

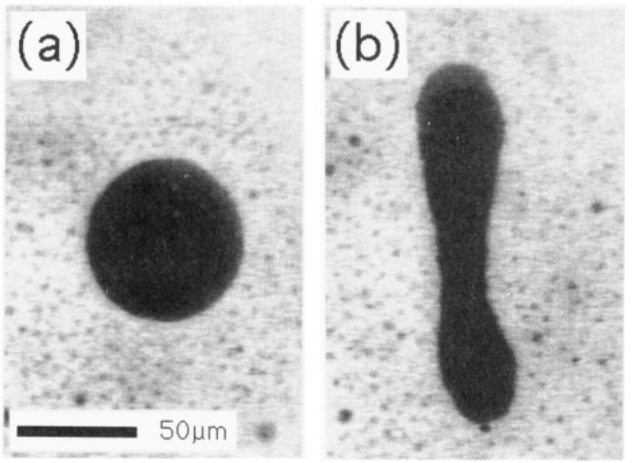


**Figure 8.** Shape transition from (a) a circular domain to (b) one with a dog-bone shape. This dog-bone shape undergoes thermal shape fluctuations but maintains an average 2-fold symmetry.

of each domain were then noted. The results from four experiments are shown in Figure 7. Results obtained from this set of experiments can be used to test the validity of the theoretical prediction of the critical domain size, $R_n$, for $n$-fold transitions given by eq 8. The theoretical values of $R_n/R_2$ are shown in the same figure as the experimental results (see Figure 7) and are found to be in good agreement within experimental errors.

A second set of experiments which gives only qualitative results was carried out. Here we monitored the shape transitions of a single large circular lipid domain held at different surface pressures. The surface pressure of the system was altered very slowly until slight distortions of the circular shape was observed. The system was then left at that particular pressure for up to 30 min for the shape distortions to develop. By changing the surface pressure slightly for the various experiments, we observed early harmonic shape distortions with different $n$-fold symmetries. The first mode to become unstable is the lowest order one with $n$ = 2, in accord with the theoretical prediction shown in Figure 2. A circular domain, as the one shown in Figure 8a, was observed to undergo harmonic shape distortions with 2-fold rotational symmetry and to ultimately attain a dog-bone shape as in Figure

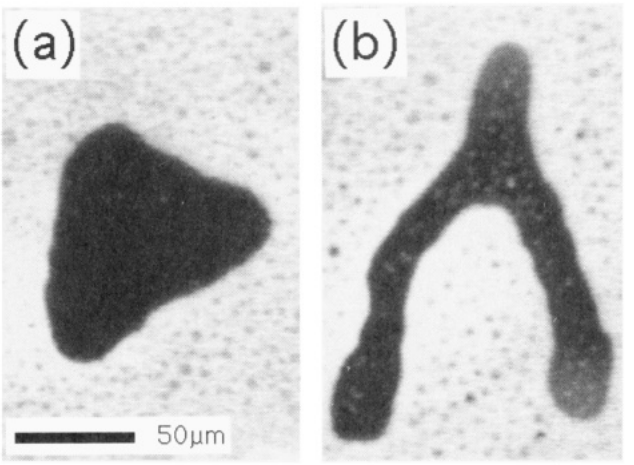


**Figure 9.** A circular domain was compressed beyond its equilibrium size and was seen to undergo a shape transition to first (a) a quasi-triangle shape and eventually to (b) a shape with three branched arms. Comparison of the experimentally observed quasi-triangle shape at the initial stage of the transition, and a shape obtained by mathematically adding a harmonic distortion to the circular shape indicates that the amplitude of distortion $r_n$ shown in (a) is approximately 17% of the radius. Using eq 43 and judging from the shape distortion of the domain at two separate instances at the initial stage of the transition, an estimate of the drag coefficient $\gamma$ was found to be on the order of 15 dyn·s/cm$^3$.

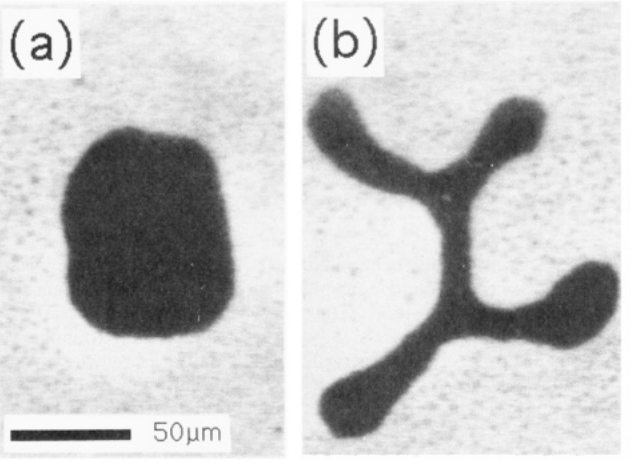


**Figure 10.** Shape transition from a circular domain to (a) an intermediate shape of a quasi-square and then to (b) a shape with four branched arms. Comparison of the experimentally observed quasi-square shape at the initial stage of the transition and a shape obtained by mathematically adding a harmonic distortion to the circular shape indicates that the amplitude of distortion $r_n$ shown in (a) is approximately 8.5% of the radius.

8b. Figures 9a, 10a, and 11a show shape transitions with 3-, 4-, and 6-fold rotational symmetries. The circular edge first transforms to an approximate straight edge of an $n$-sided quasi-polygon, as shown in the figures, which sometimes takes minutes to develop. Once a quasi-polygon is formed, the shape transition continues, developing branched patterns and taking on symmetries that are usually lower than that of the early quasi-polygon (see Figures 9b, 10b, and 11b).

In general, as the size of a domain increases ($R_c/R_{eq}$ increases), there is a switch in the symmetry of the fastest growing mode, $n^* \rightarrow n^* + 1$. From a theoretical point of view, there must be some (possibly narrow) range of $R_c/R_{eq}$ values where modes $n^*$ and $n^* + 1$ can develop simultaneously. We have sometimes observed domains with "impure" harmonic shapes that may originate in this way.

## Discussion

The observation of domain shape transitions from circles to shapes with different $n$-fold symmetries upon increase in domain

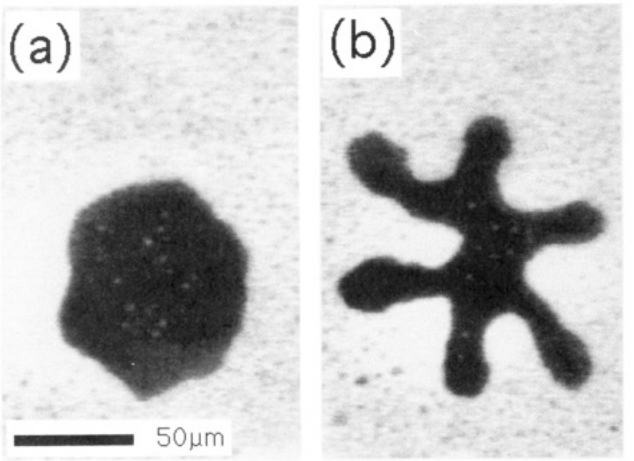


**Figure 11.** Shape transition from a circular domain to (a) an intermediate quasi-hexagon shape and then to (b) a shape with six branched arms. Comparison of the experimentally observed quasi-hexagon shape at the initial stage of the transition and a shape obtained by mathematically adding a harmonic distortion to the circular shape indicates that the amplitude of distortion $r_n$ shown in (a) is approximately 7% of the radius.

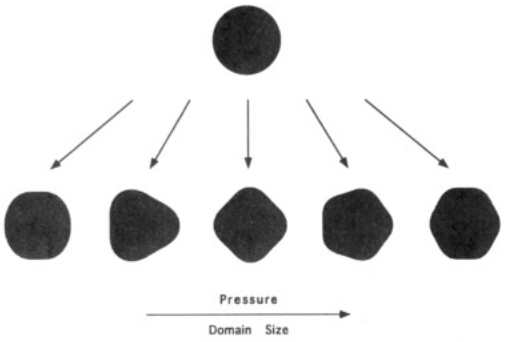


**Figure 12.** The first stage of harmonic shape transition for lipid monolayer domains. A circular domain, upon increase in pressure or domain size, undergoes a shape transition. The circular domain initially transforms to the shape of an $n$-sided quasi-polygon before proceeding to a branched shape made up of $n$ arms as observed experimentally. The quasi-polygons shown are obtained by mathematically adding harmonic distortions of different $n$-fold symmetries. The amplitude of the harmonic distortions $r_n$ for the shape with 2-fold symmetry is 20% of the radius, 12% for the shape with 3-fold symmetry, 7.5% for the shape with 4-fold symmetry, 5% for the shape with 5-fold symmetry, and 3% for the shape with 6-fold symmetry.

size or surface pressure provides evidence for the theoretical model. The attainment of the shape of a quasi-polygon in the course of the transition can be understood in terms of a competition between all different unstable modes. From the stability analysis, it is known that a circular domain of radius $R_n$ is unstable to any mode of distortion that is less than or equal to $n$. In the kinetics analysis, it is shown that the fastest growing mode $n^*$ has a lower symmetry than the critical mode $n$ ($n/n^* \approx e^{1/3}$). At the initial stage of the shape transition, all the unstable modes compete, each tending to transform the circular domain into a shape with $m$-fold symmetry where $2 < m \leq n$. With dissipation, a single mode, $n^*$, can win the competition. The early shape of this fastest growing mode appears as an $n^*$-sided quasi-polygon. The rounded vertices of the polygon continues to grow, giving rise to the branched patterns shown theoretically by Langer *et al.*[17] Figure 12 shows how a circular domain attains the shape of different quasi-polygons by mathematically adding harmonic distortions.

In our experiments (Figures 10 and 11), the quasi-polygon domains with approximate $n$-fold rotation symmetry develop into branched structures with $n$ arms, but with reduced symmetry. This loss of symmetry may be related to the initial conditions (the "negligible" $A_n$ in eq 43) that become more and more important as the domain shape develops away from a simple harmonic shape. This possibility is made clear by the work of Langer et al.,[17] who have used "noisy circles" as the initial condition in their calculations of the kinetics of shape transitions. In their calculations there is often an initial development of a simple harmonic quasi-polygon shape, followed by the formation of domain shapes with extended arms that only rarely retain the full rotational symmetry of the most unstable mode.

The loss of symmetry of the lipid monolayer domains in the experiments may arise from thermal fluctuations during the course of the shape changes. As pointed out above, the absence of a simple symmetry may also arise from a set of parameters ($R_c$, $\lambda/\mu^2$) such that there is a degeneracy or near degeneracy of the force constant $K_n$.

It is an open question as to what metastable ("excited") states exist for a given domain and whether the lowest energy states are symmetrical. In this connection, it may be noted that, for shapes with 2-fold symmetry, previous theoretical work assumed an elliptical variational function and described a second-order shape transition from a circular to an elliptical shape.[7,8,10] In the present work we have however observed the transition of a circular domain shape to a terminal dog-bone shape, with an elliptical distortion as an unstable intermediate shape.[28] Recently, numerical calculations have been carried out in this laboratory for the $n = 2$ transition using another variational function that has 2-fold symmetry (ovals of Cassini). The results of these calculations show the circle to dog-bone shape transition to be weakly first order, with a nonstationary elliptical intermediate state and a dog-bone shaped stable state.[29] It is therefore plausible that symmetrical, branched domains with $n$-fold symmetry do represent a set of energy minima for lipid domains.

**Acknowledgment.** We thank J. F. Klingler and D. J. Benvegnu for helpful discussions and assistance and R. de Koker for discussions concerning the circle to dog-bone shape transition. We acknowledge C. E. D. Chidsey for his helpful suggestions with regard to the electrical antenna. We are also indebted to R. E. Goldstein and D. P. Jackson for a preprint of their recent study on labyrinthine pattern formation in magnetic fluids. The work was supported by the National Science Foundation (Grant NSFG 9005556).

## Appendix: Comparison with Langer, Goldstein, and Jackson[17]

Lipid domains are analogous to two-dimensional domains of ferrofluids in a transverse magnetic field, which have electron spins aligned perpendicular to the plane and whose shapes are also controlled by dipolar forces and line tension.[15] Recently, Langer *et al.*[17] have developed a theory for the dynamics of pattern formation in two-dimensional ferrofluids that also applies to monolayers.[30] We compare the results of our calculations and theirs for the early kinetics of shape changes, that is, the initial departures from circular shapes.

Langer *et al.*[17] considered a slab of magnetic fluid of thickness $h$ in the $z$ direction, having a uniform cross section described by an arbitrary simple closed curve in the $xy$ plane. Ignoring second-order contributions, the energy of this system for an equivalent circular domain of radius $R_0$ is

$$E = -2\pi\mu^2 R_0 \ln \frac{8R_0}{e^{1/2}h} + 2\pi R_0 \lambda_0 \qquad (45)$$

In their formulation, the line tension $\lambda_0$ used is the bare line tension, which is related to the effective line tension $\lambda$ by eq 4, while $R_0 = (A/\pi)^{1/2}$ is the equivalent radius of an arbitrarily-shaped slab of area $A$. Assuming that the slab height is related to the dipole–dipole separation distance by

$$h = e^{1/2}\Delta \qquad (46)$$

it can be seen that the energy shown in eq 45 is identical to the one we obtained for a circular lipid domain (see eq 5).

In the stability analysis carried out for the ferrofluids, the growth rate of the domain of mode $n$, $\sigma_n$, was found to be

$$\left(\frac{R_0^2}{\lambda_0}\right)\sigma_n = 1 - n^2 + \frac{\mu^2}{\lambda_0}\left\{(n^2-1)\left[1 + \ln\left(\frac{2R_0}{h}\right) - C\right] - n^2 \ln n\right\} \quad (47)$$

where $C$ is the Euler constant. In the limit of large $n$ and with the substitution of eqs 4 and 46, the critical spatial frequency, $k_{cn}$, corresponding to the highest spatial frequency for which there is an instability, is found to be identical to that obtained for a lipid domain with a straight edge (see eq 9).

The results from the dynamic instability analysis differ. In the high harmonics limit for the case of the ferrofluids, the spatial frequency of the critical mode, $k_{fc} = 2(he^{C-1}e^{\lambda_0/\mu^2})^{-1}$, was found to be larger than that of the fastest growing mode, $k_{fm} = 2(he^{C-1/2}e^{\lambda_0/\mu^2})^{-1}$, by a factor of $e^{1/2}$. In our analysis, the critical mode has a spatial frequency larger than that of the fastest growing mode by a factor of $e^{1/3}$ (see eq 44). This small difference arises from the different handling of viscous dissipation, as discussed below.

Langer *et al.*[17] examined the shape evolution of a closed curve, considering a "line dissipation" of the contour. This, as pointed out in their paper, is the simplest form one can use for a dissipation function; a more complete calculation for monolayers should include viscous dissipation at all points inside and outside the closed curve. In our analysis, we have included dissipation at all points in the two-dimensional space by considering an "area dissipation" but have grossly oversimplified the problem of the hydrodynamics of the subphase, except possibly for very shallow subphases. Although the same assumption that the viscous forces are linear in the velocity is made in both analysis, the expressions used in the integrand of the disspative energy are different. Langer *et al.* used $\gamma(\partial r/\partial t)^2$, with $r$ representing the closed curve for the domain, whereas we use $\gamma(\nabla\varphi)^2$ in the integrand of eq 41, which gives a rate of energy dissipation (per solid angle) term $\gamma(dr_n/dt)^2R_c^2/n$. This energy dissipation term has an explicit $1/n$ dependence, which is responsible for the fact that the most rapidly growing mode is not the lowest energy mode in our analysis.

To check the significance of this $1/n$ dependence, we drop it from the energy dissipation term and carry out a similar calculation for the fastest growing mode. The resulting harmonic distortion then grows as

$$r_n = A_n \exp\left(-\frac{K_n}{\gamma R_c^2}t\right) \quad (48)$$

so that the most rapidly growing mode is the lowest energy mode (see Figure 4b). Comparison of parts a and b of Figure 4 shows that, for a domain of fixed size, the fastest growing mode has a lower symmetry when the $n$ dependence is omitted. Further analysis shows that, in the absence of the $n$ dependence, the spatial frequency ratio between the critical and the fastest growing mode shifts from $e^{1/3}$ for domains with low-order harmonic distortions to $e^{1/2}$ for domains with high-order harmonic distortions (see squares in Figure 5). The $e^{1/2}$ ratio in the high $n$ limit coincides with that of Langer *et al.*[17] Unfortunately, we cannot resolve the difference of the factor $e^{1/2}$ and $e^{1/3}$ experimentally.

After this paper was written, we obtained a preprint by Jackson and Goldstein[31] in which the work of Langer *et al.*[17] was elaborated to include a more realistic description of the hydrodynamics of thin ferrofluids. This treatment yields an $n$ dependence of the growth rate similar to that obtained in the present work.

## References and Notes


(1) Subramaniam, S.; McConnell, H. M. *J. Phys. Chem.* **1987**, *91*, 1715–1718.
(2) Rice, P. A.; McConnell, H. M. *Proc. Natl. Acad. Sci. U.S.A.* **1989**, *86*, 6445–6448.
(3) Seul, M.; Sammon, J. *Phys. Rev. Lett.* **1990**, *64* (16), 190–196.
(4) Hirshfeld, C. L.; Seul, M. *J. Phys. (Paris)* **1990**, *51*, 1537–1552.
(5) Andelman, D.; Brochard, F.; deGennes, P. G.; Joanny, J. *C.R. Acad. Sci. Paris Ser. C* **1985**, *301*, 675–678.
(6) Andelman, D.; Brochard, F.; Joanny, J. *J. Chem. Phys.* **1987**, *86*, 3673–3681.
(7) Keller, D. J.; Korb, J. P.; McConnell, H. M. *J. Phys. Chem.* **1987**, *91*, 6417–6422.
(8) McConnell, H. M.; Moy, V. T. *J. Phys. Chem.* **1988**, *92*, 4520–4525.
(9) McConnell, H. M. *J. Phys. Chem.* **1990**, *94*, 4728–4731.
(10) Vanderlick, T. K.; Möhwald, H. *J. Phys. Chem.* **1990**, *94*, 886–890.
(11) Deutch, J. M.; Low, F. E. *J. Phys. Chem.* **1992**, *96*, 7097–7101.
(12) McConnell, H. M. *J. Phys. Chem.* **1992**, *96*, 3167–3169.
(13) Flörsheimer, M. Ph.D. Thesis, Technical University of Munich, 1989.
(14) Seul, M. *J. Phys. Chem.* **1993**, *97*, 2941–2945.
(15) Rosensweig, R. E. *Ferrohydrodynamics*; Cambridge University Press: Cambridge, 1985; p 1987.
(16) Cébers, A. O.; Maiorov, M. M. *Magnetohydrodynamics* **1980**, *16*, 21–28.
(17) Langer, S. A.; Goldstein, R. E.; Jackson, D. P. *Phys. Rev. A* **1992**, *46* (8), 4894–4904.
(18) Benvegnu, D. J.; McConnell, H. M. *J. Phys. Chem.* **1993**, *97*, 6686–6691.
(19) McConnell, H. M.; de Koker, R. *J. Phys. Chem.* **1992**, *96*, 7101–7103.
(20) Thiele, A. A. *Bell System Tech. J.* **1969**, *48*, 10, 3287–3335.
(21) A similar stability–instability plot has been obtained by Langer *et al.* (see ref 17).
(22) The assumption of irrotational flow in the monolayer implies an equivalent irrotational flow in the aqueous subphase. This should be a good approximation for very shallow troughs. In our experiments the monolayer itself provides the driving force for flow, while the aqueous subphase together with the bottom of the trough provides the source of drag. For a discussion of irrotational flow in thin fluid regions, see: Batchelor, G. K. *An Introduction to Fluid Mechanics*; Cambridge University Press: Cambridge, 1967; pp 219–224.
(23) Lamb, H. *Hydrodynamics*; Dover: New York, 1945; p 471.
(24) Hughes, B. D.; Pailthorpe, B. A.; White, L. R. *J. Fluid Mech.* **1981**, *110*, 349–372.
(25) Klingler, J. F.; McConnell, H. M. *J. Phys. Chem.* **1993**, *97*, 6096–6100.
(26) Klingler, J. F.; McConnell, H. M. *J. Phys. Chem.* **1993**, *97*, 2962–2966.
(27) Heckl, W. M.; Miller, A.; Möhwald, H. *Thin Solid Films* **1988**, *159*, 125–132.
(28) Seul and Sammon have reported elliptical shapes of domains in binary mixtures of phospholipid and cholesterol near the critical composition and pressure (see ref 3). We attribute their inability to observe a circle to dog-bone shaped transition to the trapping of large phospholipid-rich (bright) domains in the cholesterol-rich (dark) domains under observation. The presence of these contaminating large domains of a second phase hinders the formation of the waist of the dog-bone shape due to the electrostatic repulsion between the trapped bright domains and the surrounding liquid phase outside the dark domain monitored. To test this effect, we have carried out experiments under similar conditions using a binary mixture of DMPC and DChol and have observed elliptical shapes similar to those reported by Seul and Sammon.
(29) de Koker, R.; McConnell, H. M. Submitted for publication.
(30) While there are many close similarities between properties of these ferromagnetic films and lipid monolayers, the two systems have significant differences. The most important of these is that in the monolayer systems the condition for equilibrium involves equalities of chemical potentials in coexisting phases. Under nonequilibrium conditions, the area of a monolayer domain need not be constant. The implicit assumption in the present paper is that the rate of domain shape change is much larger than the rate of domain area change.
(31) Jackson, D. P.; Goldstein, R. E. *Science*, in press.